Supplementary Figure Legends

Supplementary Figure 1: Neurolucida reconstructions of *Sst*-INs

Neurolucida reconstructions of representative biocytin-filled *Sst*-INs. Whole cell patch clamp recorded soma in O/A. Axon is shown in gray, and the dendrites are shown in black. All scale bars represent 100 µm. (Subi. = subiculum).

Supplementary Figures 2: Spatial distribution analysis of the transcriptomic dataset

Top 25 hits minimizing for spatial dispersion for pairs of genes (shown above maps) combined with *Sst*. Multiple genes fit the criteria and could in principle be used. Underlined genes identify genes for which transgenic mouse models exist.

Supplementary Figure 3: Spatial distribution analysis of the transcriptomic dataset, continued

Next 25 hits in the spatial distribution analysis shown in Fig. S2.

Supplementary Figure 4: Neurolucida reconstructions of *Sst;;Tac1*-INs

Neurolucida reconstructions of biocytin-filled *Sst;;Tac1*-INs. Axon is shown in green, and the dendrites are shown in black. All scale bars represent 100 µm. The CA2 to CA1 border (determined visually by the change in pyramidal cell layer compactness) is shown by dashed lines in the 3 cells where a CA2 projection was found.

Supplementary Figure 5: Neurolucida reconstructions of *Ndnf;;Nkx2-1*-INs

Neurolucida reconstructions of biocytin-filled *Ndnf;;Nkx2-1*-INs. Axon is shown in orange, and the dendrites are shown in black. All scale bars represent 100 µm.

Supplementary Figure 6: Neurolucida reconstructions of *Chrna2*-INs

Neurolucida reconstructions of biocytin-filled *Chrna2*-INs. Axon is shown in blue, and the dendrites are shown in black. All scale bars represent 100 µm.

Supplementary Figure 7: Neurolucida reconstructions of *Sst;;Nos1*-INs

Neurolucida reconstructions of biocytin-filled *Sst;;Nos1*-INs. Axon is shown in magenta, and the dendrites are shown in black. All scale bars represent 100 µm. For cells found to project to subiculum (Subi.), the termination of the pyramidal cell layer is shown, and subiculum is indicated.

Supplementary Figure 8: Axonal and dendritic distributions

A, Cumulative axonal distribution for all neurons recorded, alternative representation to Fig. 1H Number of cells: *Sst* = 21; *Sst;;Tac1* = 25; *Ndnf;;Nkx2-1* = 15; *Chrna2* = 19; *Sst;;Nos1* = 15. **B**, Cumulative dendritic distribution for all neurons recorded. Number of cells: *Sst* = 21; *Sst;;Tac1* = 26; *Ndnf;;Nkx2-1* = 18; *Chrna2* = 21; *Sst;;Nos1* = 14.

Supplementary Figure 9: Analysis of electrophysiological parameters used for clustering

A – E, Cumulative distributions of AP threshold (A), AP amplitude (B), AP full width at half maximum (C), rebound depolarization amplitude (D), and sag amplitude (E) for all neurons recorded in this study. The coefficient of variation measured across all neurons is shown below each graph. The combination of these 5 parameters and the 3 parameters reported in Figure 2 were used for the cluster analysis.

Supplementary Figure 10: Optogenetic circuit mapping using Cs^+ internal solution

A, Examplar voltage-clamp recordings (0 mV) form the postsynaptic neurons showing inhibitory currents evoked by optogenetic stimulation (20 ms) of the different *Sst*-IN subtypes. With Cs^+-based intracellular solution, postsynaptic targets were easily identified as CA1-PYRs or interneurons based on their shape and location. Putative PV-INs were identified as large vertically oriented neurons at the PYR/Oriens border, while putative SST-INs were identified as horizontally oriented neurons at the Oriens/Alveus border. Overall, putative PV-INs had significantly lower input resistance (112.5 ± 6 MΩ; n = 36) than putative SST-INs (185.5 ± 18.6 MΩ; n = 22; p <

0.001, unpaired t-test). **B**, Summary bar graph showing IPSC amplitude evoked by photostimulation of the 4 genotypes. Optogenetic stimulation of *Sst;;Tac1*-INs revealed large amplitude inhibitory postsynaptic currents (IPSCs) in putative PV-INs (151 ± 26.2 pA, n = 13) but significantly smaller IPSCs in CA1-PYRs (54.8 ± 13.2 pA; n = 15; $p < 0.001$, Mann Whitney U test) and putative SST-INs (20.8 ± 7.7 pA; n = 3; $p < 0.01$, Mann Whitney U test). In contrast, photostimulation of Ndnf;;Nkx2-1-INs generated significantly larger IPSCs in CA1-PYRs (86.8 ± 10.3 pA; n = 16) than in putative PV-INs (21.3 ± 10.9 pA; n = 12; $p < 0.001$, Mann Whitney U test) or putative SST-INs (2.9 ± 2 pA; n = 5; $p < 0.01$, Mann Whitney U test). On the other hand, optogenetic stimulation of *Chrna2*-INs resulted in IPSCs of similar average amplitude in CA1-PYRs (69.1 ± 10.9 pA; n = 14) and putative PV-INs (72.9 ± 40.3 pA; n = 9; but for which the difference was statistically significant, $p < 0.05$, Mann Whitney U test). IPSCs recorded in putative SST-INs (1.6 ± 0.9 pA; n = 6) where smaller than IPSCs recorded in both CA1-PYRs and putative PV-INs ($p < 0.001$ vs. CA1-PYRs and $p < 0.01$ vs. putative PV-INs, Mann Whitney U test). Finally, photostimulation of *Sst;;Nos1*-INs revealed almost undetectable IPSCs in the three targets (CA1-PYRs: 1.7 ± 0.9 pA; n = 12; putative PV-INs: 1.1 ± 1 pA, n = 6; putative SST-INs: 0.5 ± 0.4 pA, n = 8). Average ± SEM is shown.

Supplementary Figure 11: Neurolucida reconstructions of *Pv*-INs

Neurolucida reconstructions of biocytin-filled *Pv*-INs. Axon is shown in red, and the dendrites are shown in black. All scale bars represent 100 µm.

Supplementary Figure 12: Differential effect of repetitive Schaffer collaterals' stimulation on the 6 interneuron populations

A – F, Current-clamp recordings in which Schaffer collaterals were stimulated at 5 X 50 Hz (arrowheads) for the 6 interneuron populations investigated. Examples show 10 consecutive sweeps. Graphs showing the action potential probability as a function of stimulus number. Thin lines show individual neurons, and the bold lines show their average ± SEM (as reported in Fig. 5C). Number of cells reported correspond to Fig. 5C.

Supplementary Figure 13: Dissection of the current-clamp waveforms during repetitive Schaffer collaterals' stimulation and intrinsic membrane properties

A, Peak EPSP amplitude as a function of stimulus number. **B**, Feed-forward EPSP amplitude as a function of stimulus number. **C**, Feed-back EPSP amplitude as a function of stimulus number. Number of cells analyzed in A – C correspond to that reported in Fig. 5C. **D, E**, Input resistance (D) and membrane time constant (E) for the different genotypes. *Sst;;Tac1*-INs demonstrated similar input resistance when compared with other subtypes (*Sst;;Tac1*-INs: 138.3 ± 9.5 MΩ; n = 16; *Sst*-INs 111 ± 5.9 MΩ; n = 20; p > 0.05; *Ndnf;;Nkx2-1*-INs: 117.7 ± 5.2 MΩ; n = 15; p > 0.1; *Chrna2*-INs: 149.4 ± 12.6 MΩ; n = 12; p > 0.1; *Sst;;Nos1*-INs: 230.3 ± 34.4 MΩ; n = 12; p > 0.05. P-values for the comparison of *Sst;;Tac1*-INs with other genotypes. P-values were corrected with Holm-Bonferroni method for multiple comparisons. *Sst;;Tac1*-INs demonstrated faster membrane time constant than most other subtypes (*Sst;;Tac1*-INs: 19.2 ± 2.3 ms; n = 16; *Sst*-INs 29.3 ± 1.8 ms; n = 20; p < 0.01; *Ndnf;;Nkx2-1*-INs: 26.4 ± 1.5 ms; n = 15; p < 0.05; *Chrna2*-INs: 26.7 ± 2.7 ms; n = 12; p = 0.07; *Sst;;Nos1*-INs: 66 ± 10.5 ms; n = 12; p < 0.01. P-values for the comparison of *Sst;;Tac1*-INs with other genotypes. P-values were corrected with Holm-Bonferroni method for multiple comparisons.

Supplementary Figure 14: Voltage-clamp recordings during repetitive Schaffer collaterals' stimulation

A1 – A4, Voltage-clamp recordings at -60 mV from the four *Sst*-INs subtypes. **B**, Peak EPSC amplitude as a function of stimulus number. EPSC facilitation in *Ndnf;;Nkx2-1*-INs was less monotonic than in *Chrna2*-INs, and *Sst;;Nos1*-INs demonstrated initially facilitating EPSP/Cs which then depressed, all consistent with the recruitment of these cells in current-clamp experiments. **C**, Feed-forward EPSC amplitude as a function of stimulus number. Only *Sst;;Tac1*-INs and *Sst;;Nos1*-INs demonstrated FF EPSCs in response to Schaffer collaterals' stimulation. **D**, Cumulative charge as a function of stimulus number. *Sst;;Tac1*-INs and *Sst;;Nos1*-INs had larger cumulative charge initially, but the extensive short-term facilitation of EPSCs in *Ndnf;;Nkx2-1*-INs and *Chrna2*-INs eventually resulted in similar cumulative charge across all subtypes. Average ± SEM shown in panels B – D. Number of cells analyzed in B, C and D: *Sst;;Tac1*-INs = 7; *Ndnf;;Nkx2-1*-INs = 9; *Chrna2*-INs = 6; *Sst;;Nos1*-INs = 10.

Supplementary Table 1: p-values for statistical comparisons of anatomical parameters

P-values reported for Kolmogorov-Smirnov tests followed by Holm-Bonferroni correction performed on data reported in Figure S8.

Supplementary Table 2: p-values for statistical comparisons of electrophysiological parameters

P-values reported for Kolmogorov-Smirnov tests followed by Holm-Bonferroni correction for data presented in Figure 2D – F and Figure S9.

Supplementary Table 3: Contribution of individual parameters to the principal components

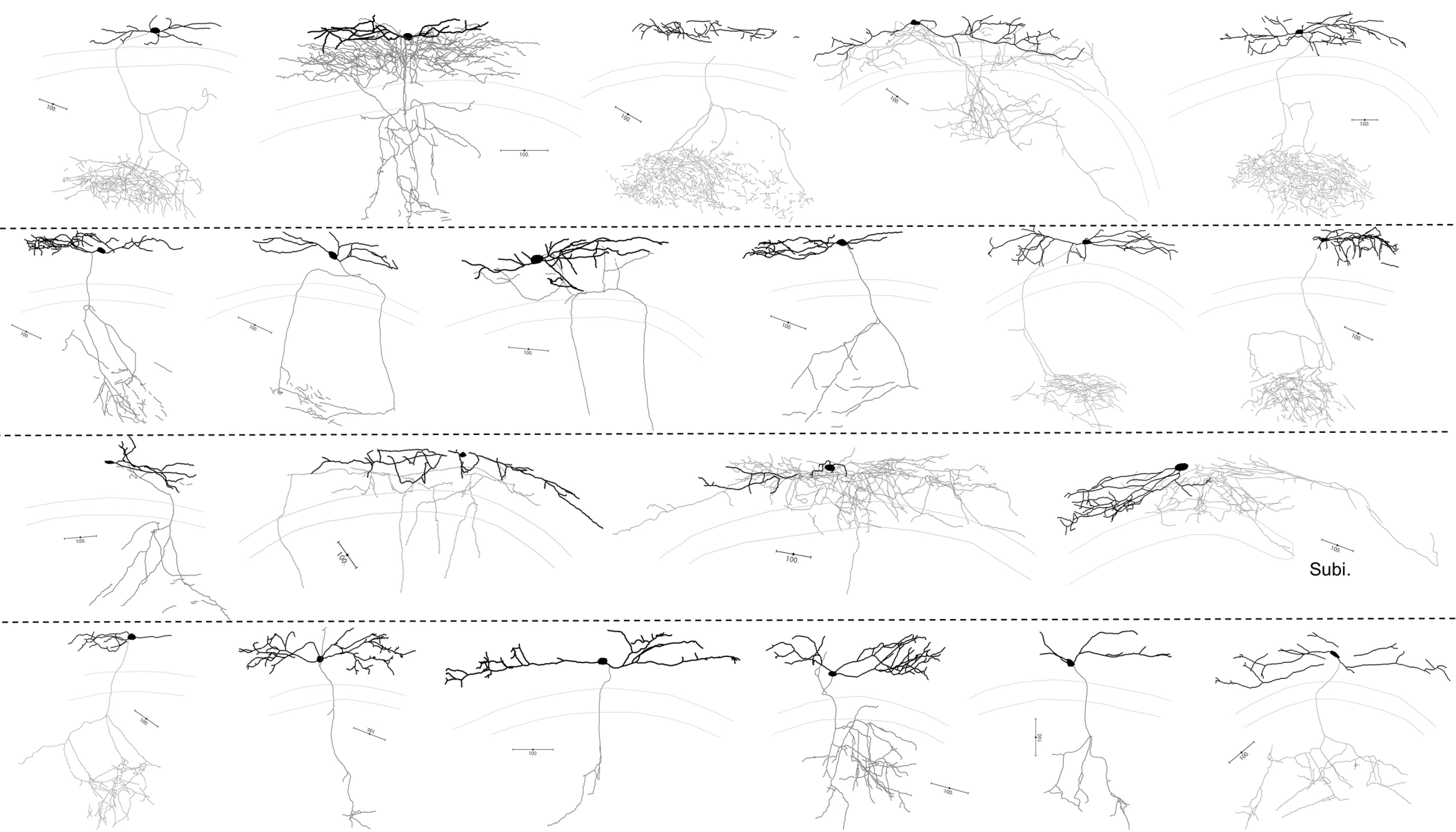

Supplementary Figure 1

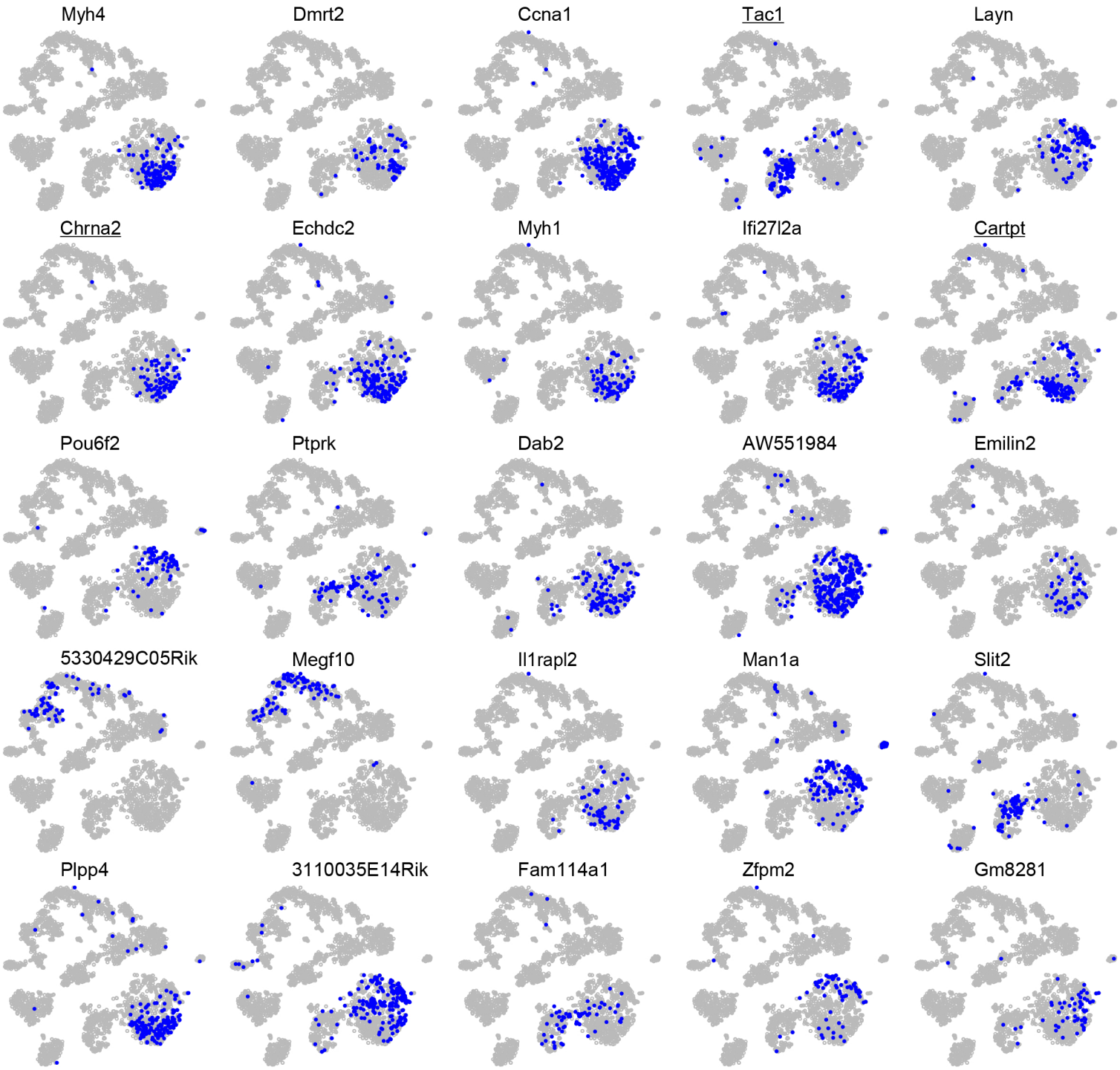

Supplementary Figure 2

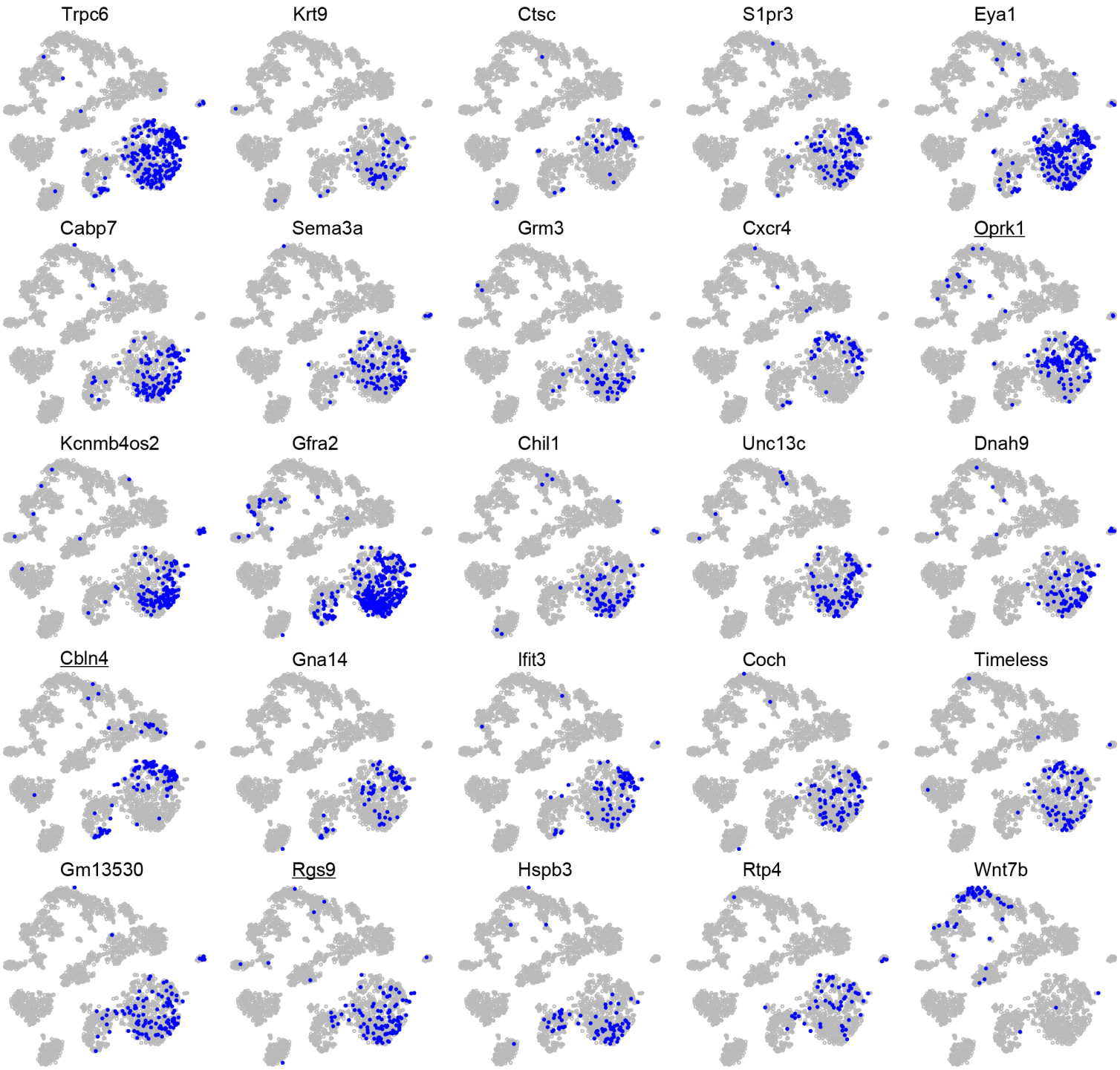

Supplementary Figure 3

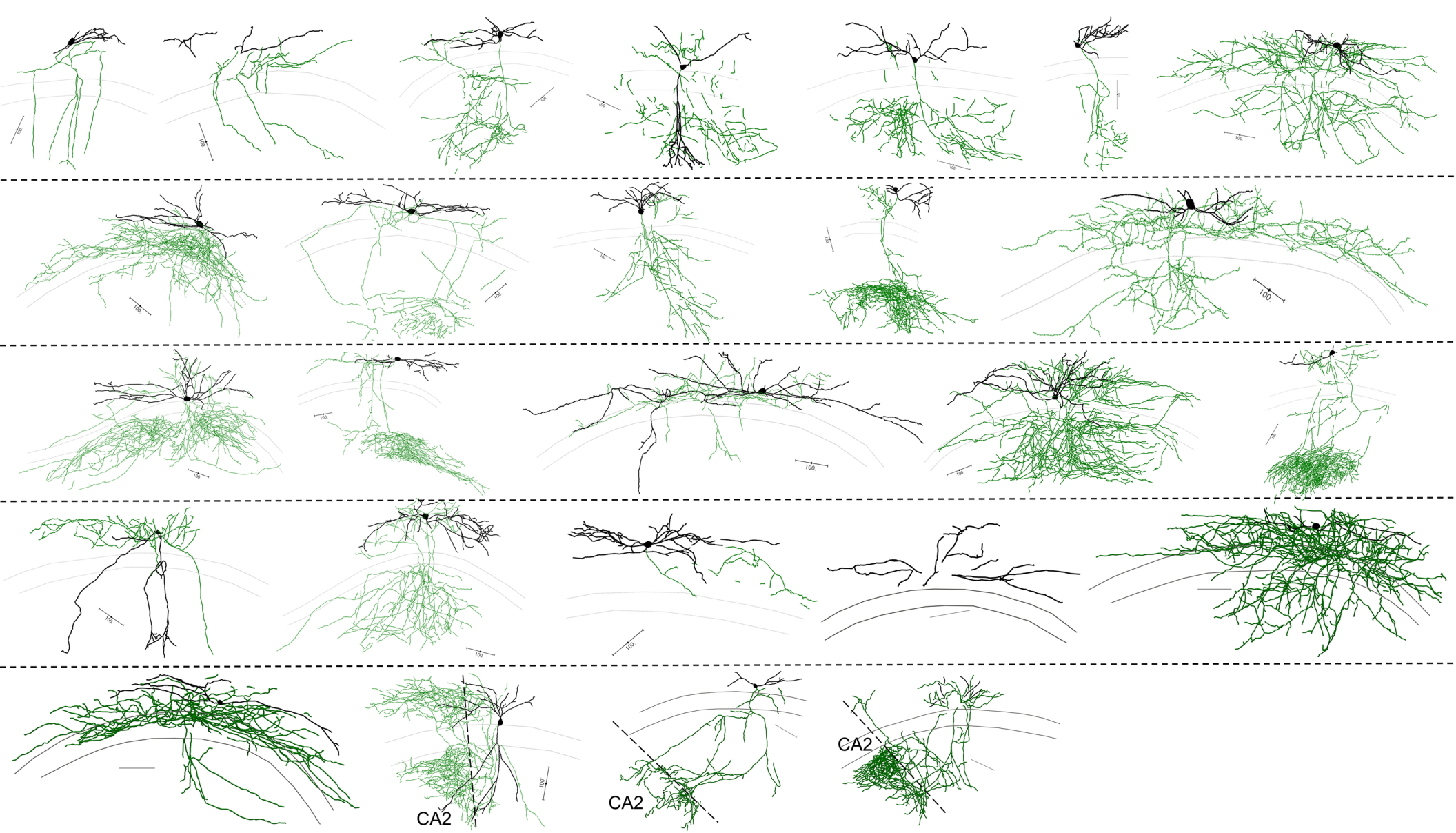

Supplementary Figure 4

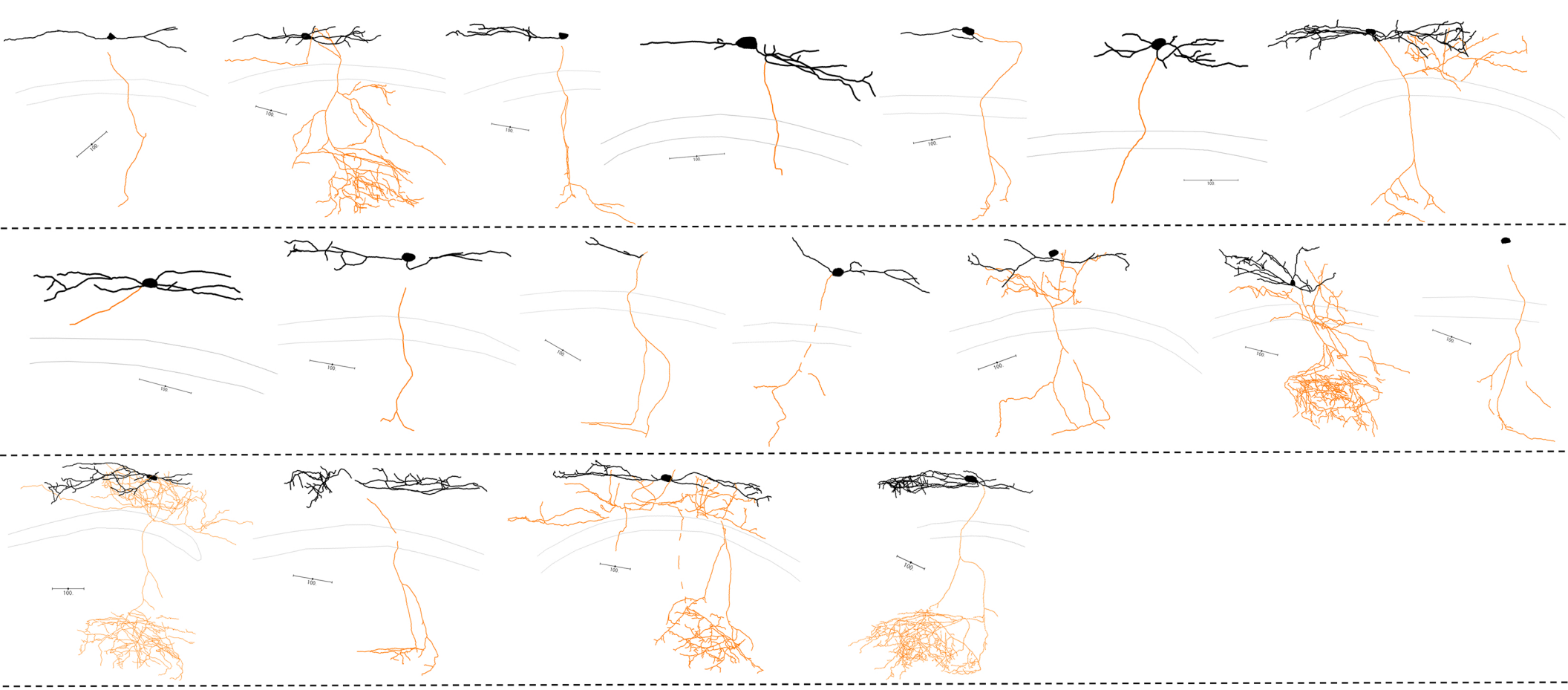

Supplementary Figure 5

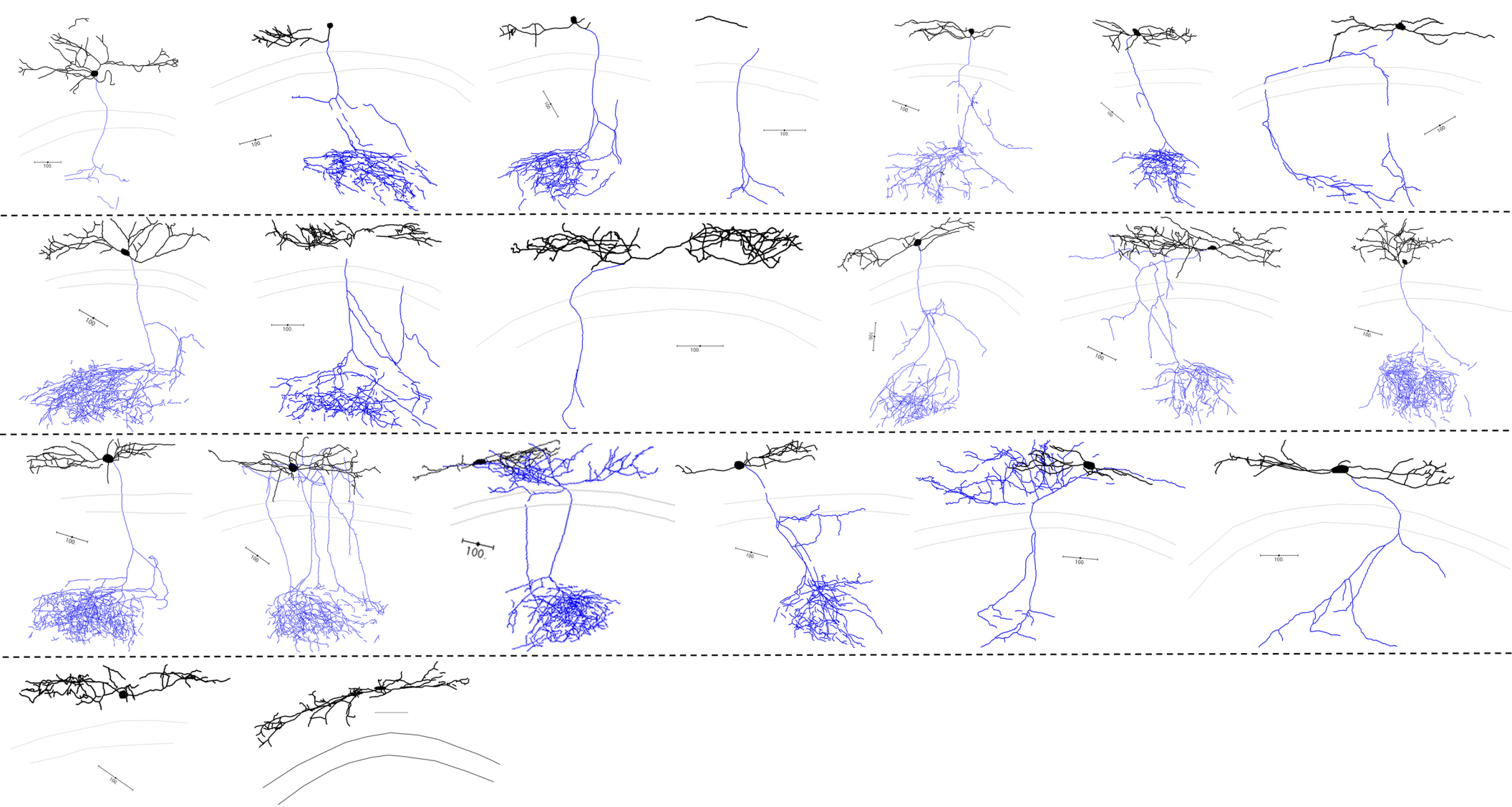

Supplementary Figure 6

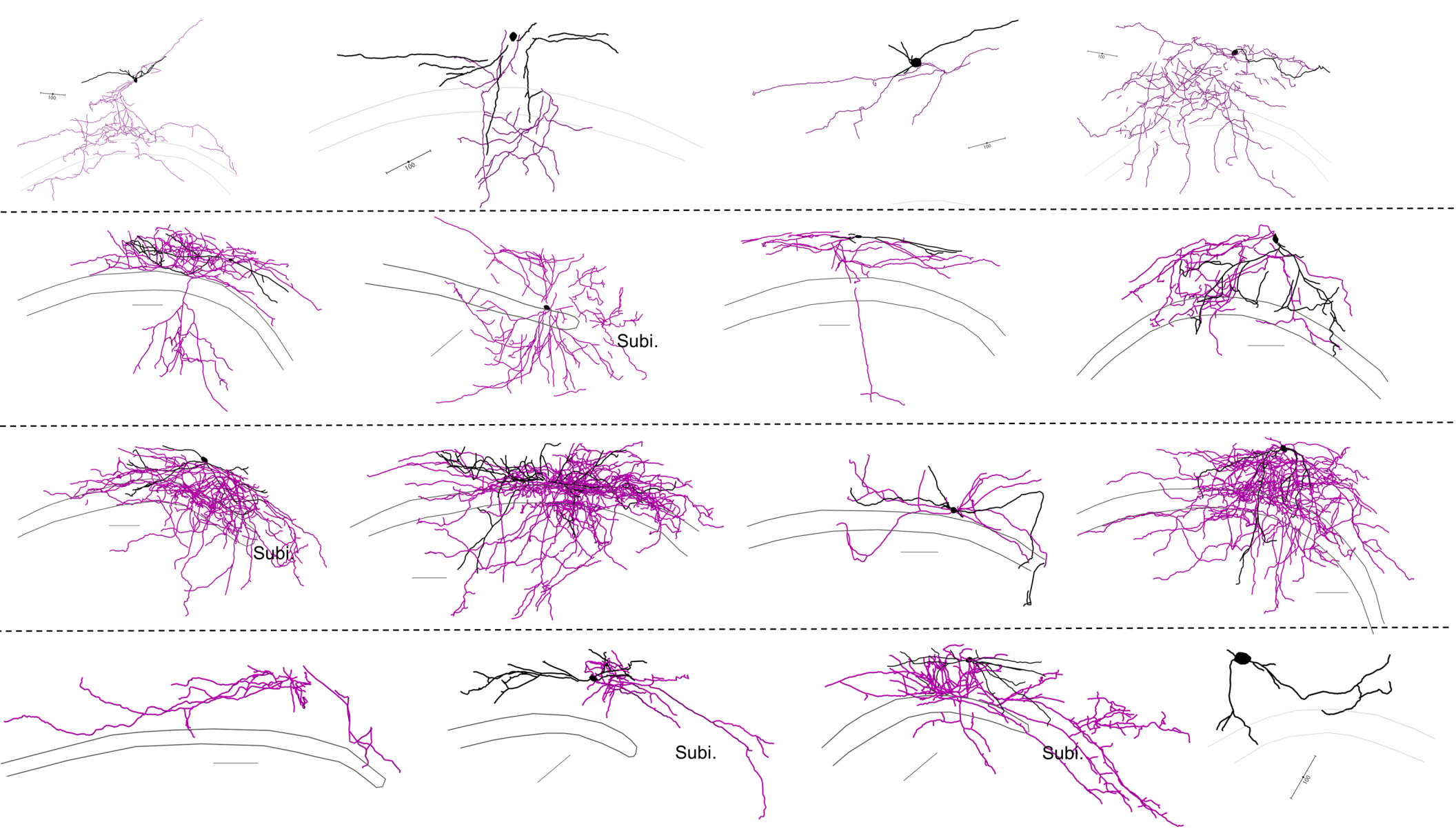

Supplementary Figure 7

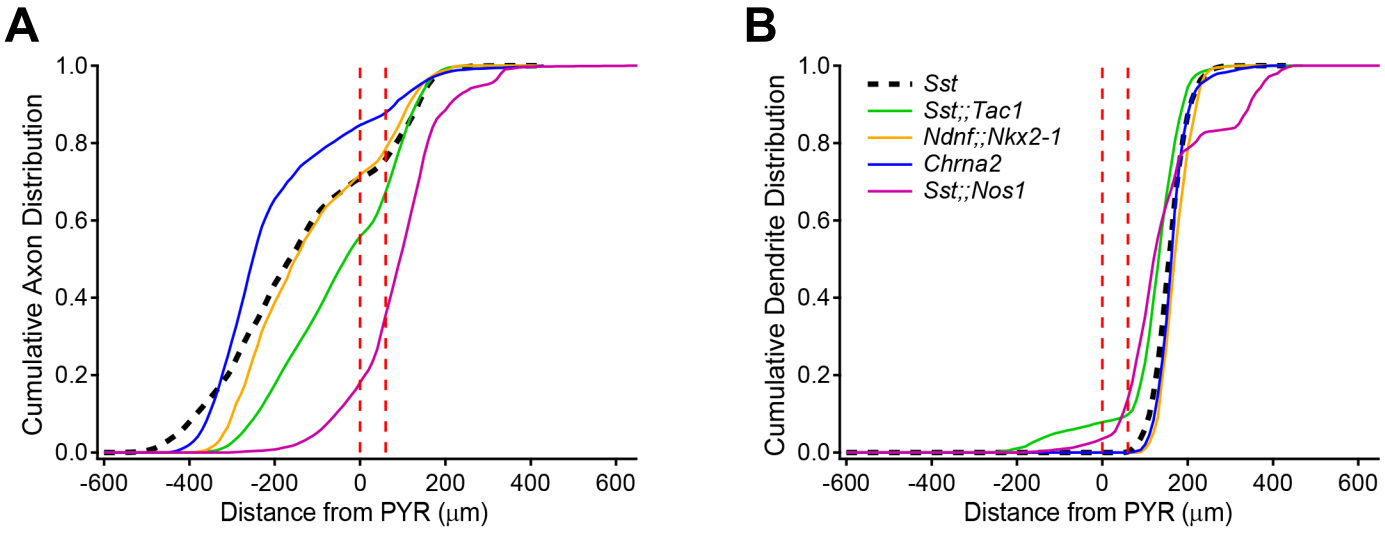

Supplementary Figure 8

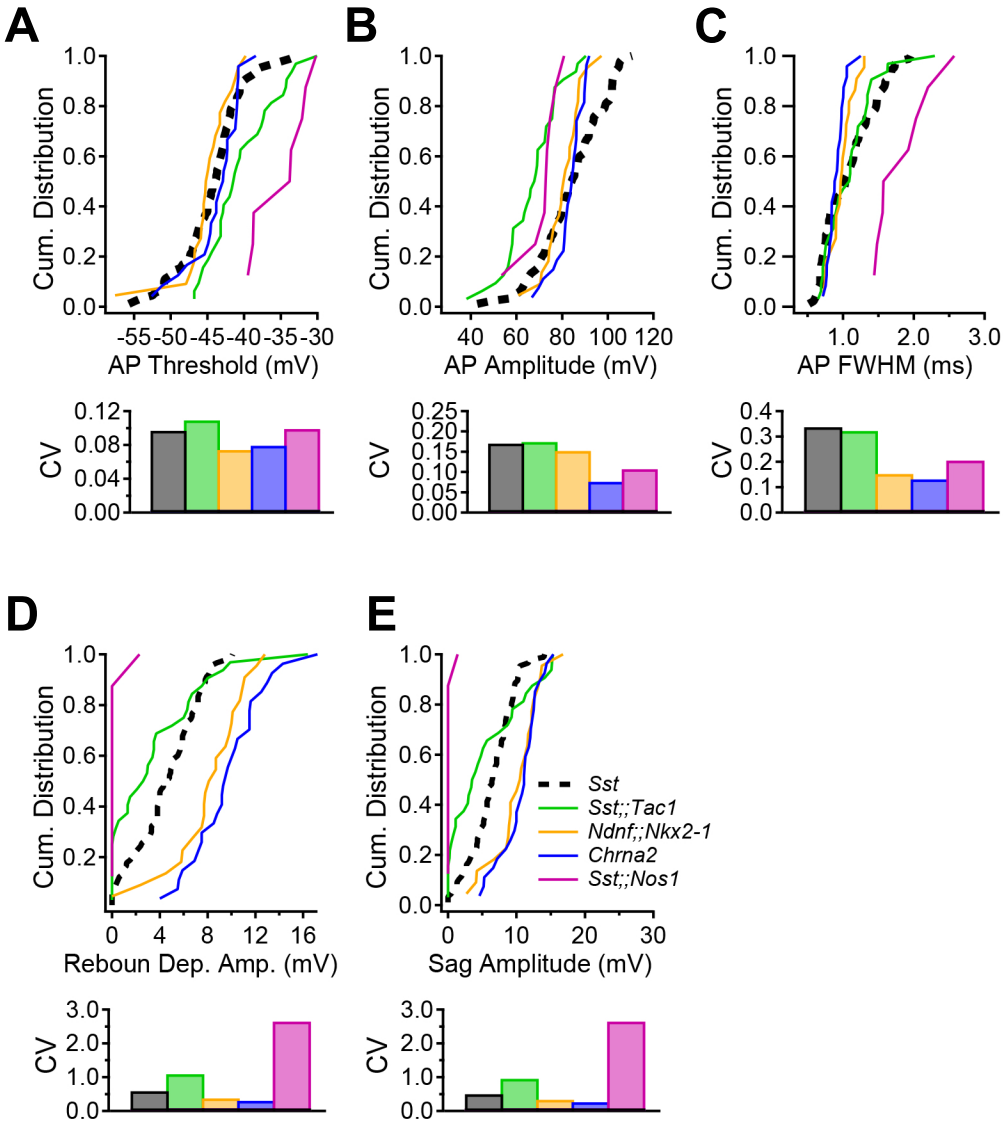

Supplementary Figure 9

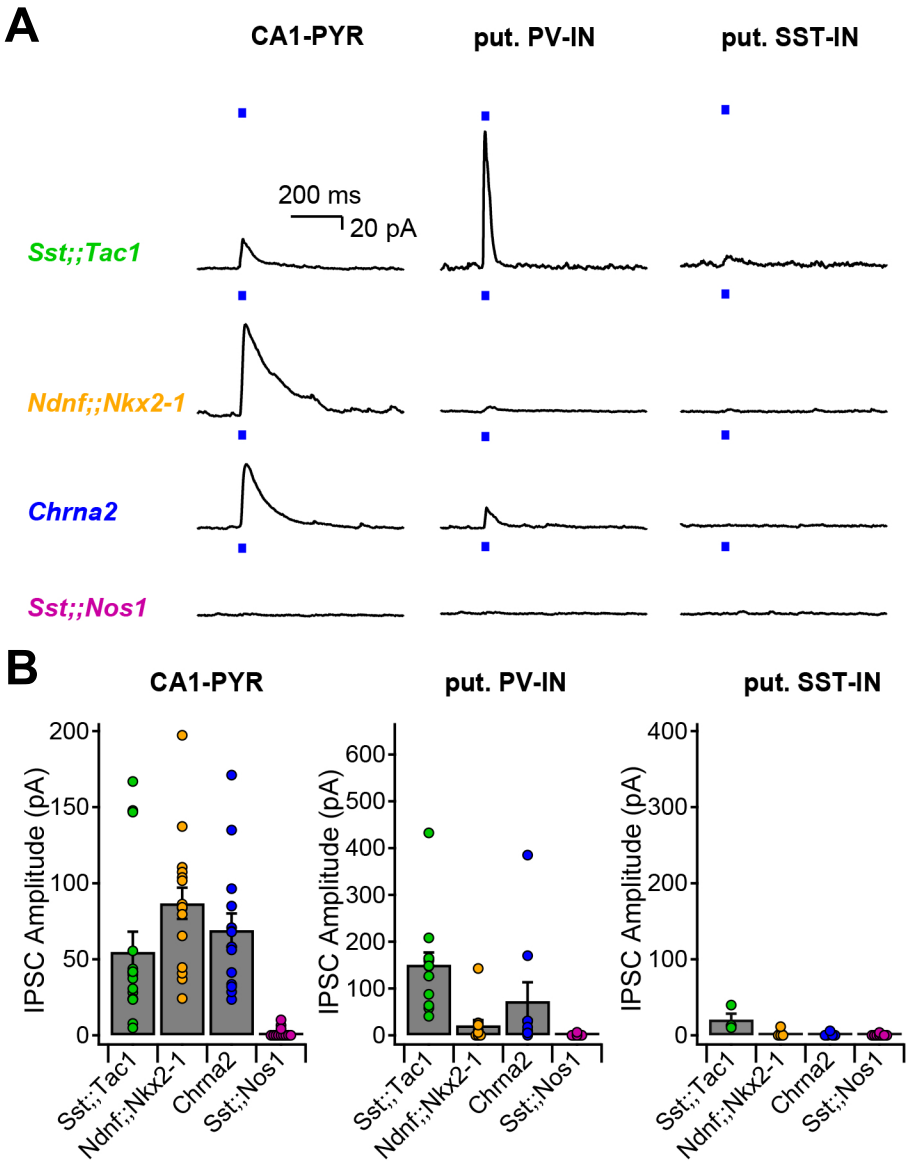

Supplementary Figure 10

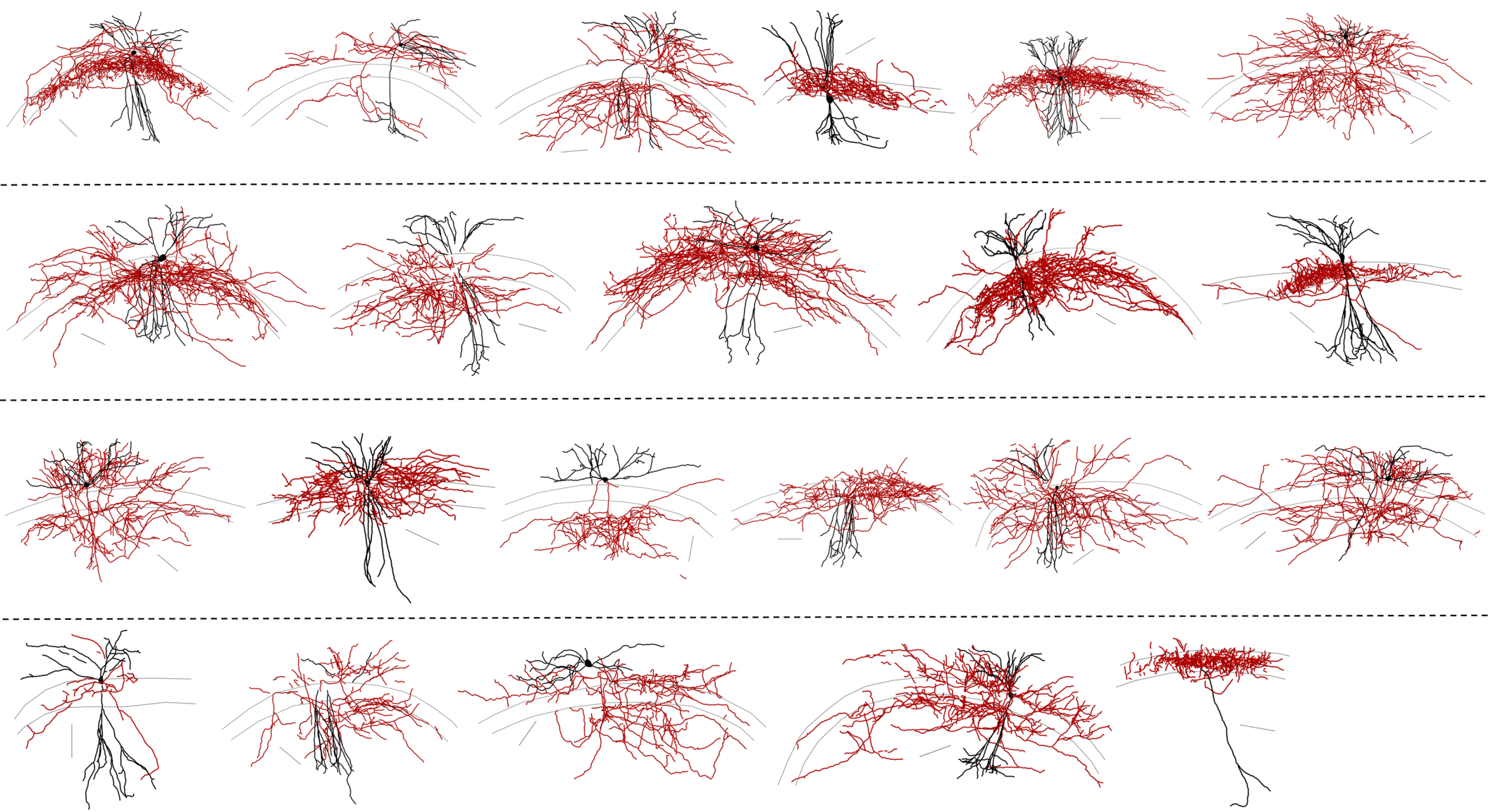

Supplementary Figure 11

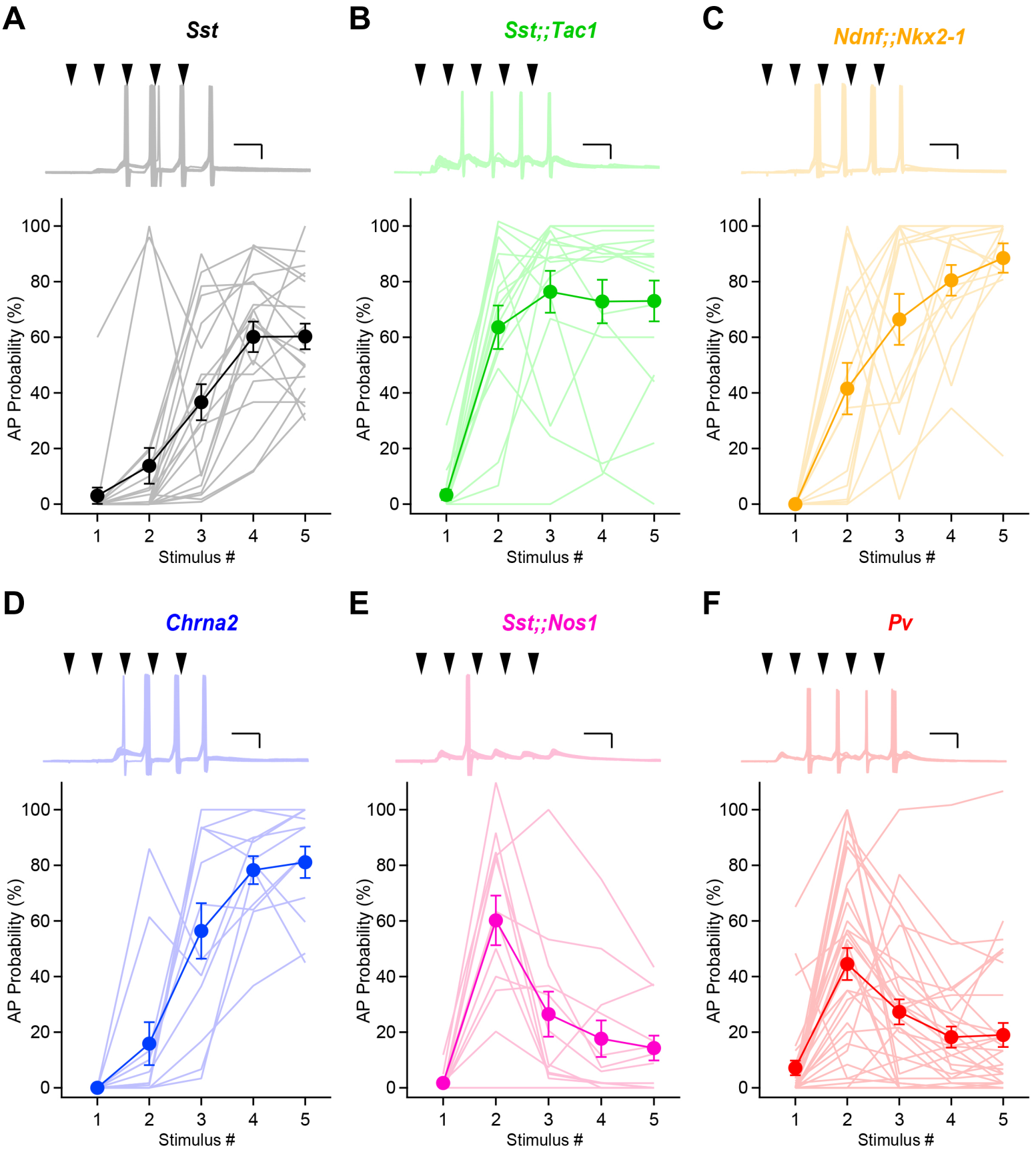

Supplementary Figure 12

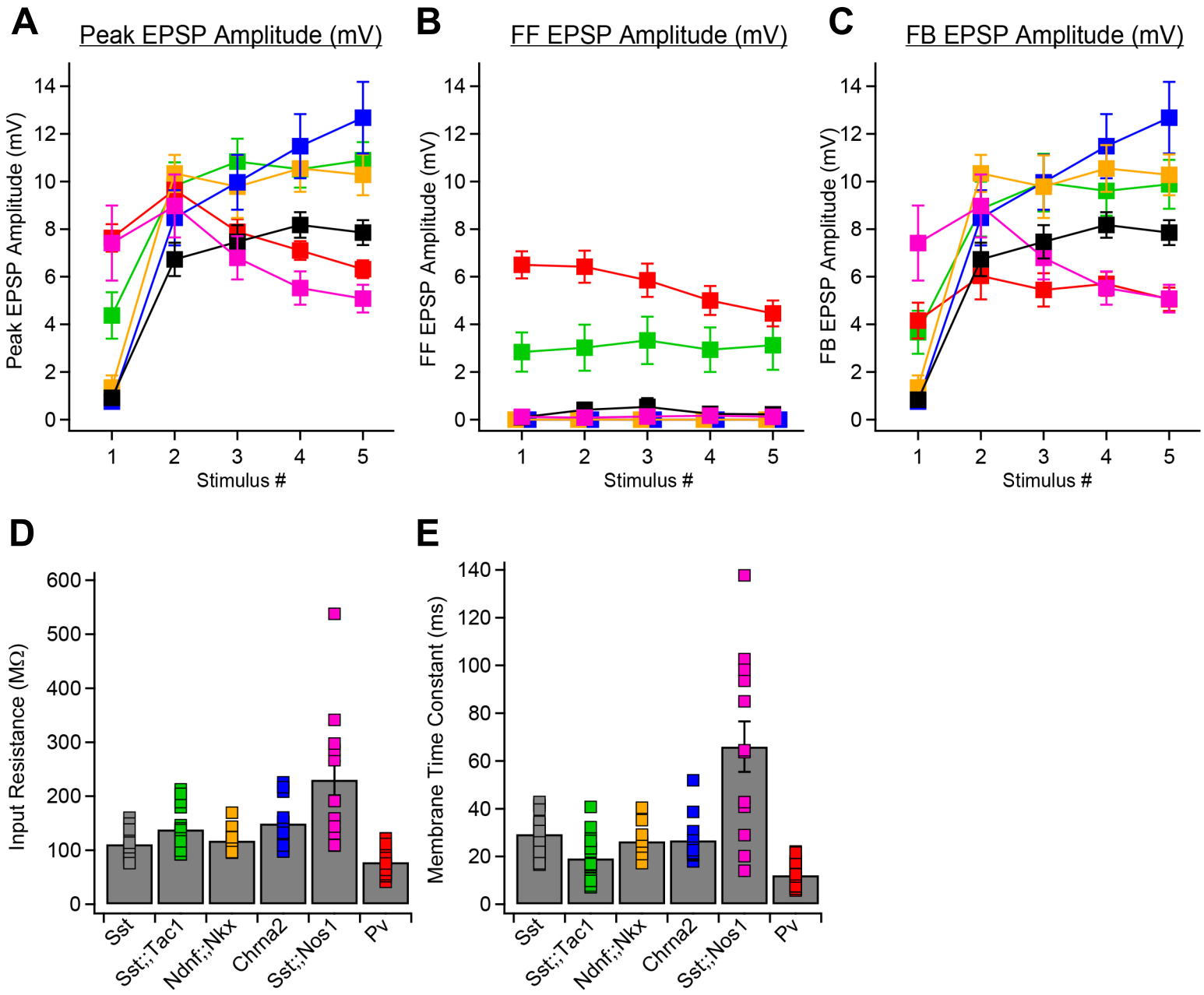

Supplementary Figure 13

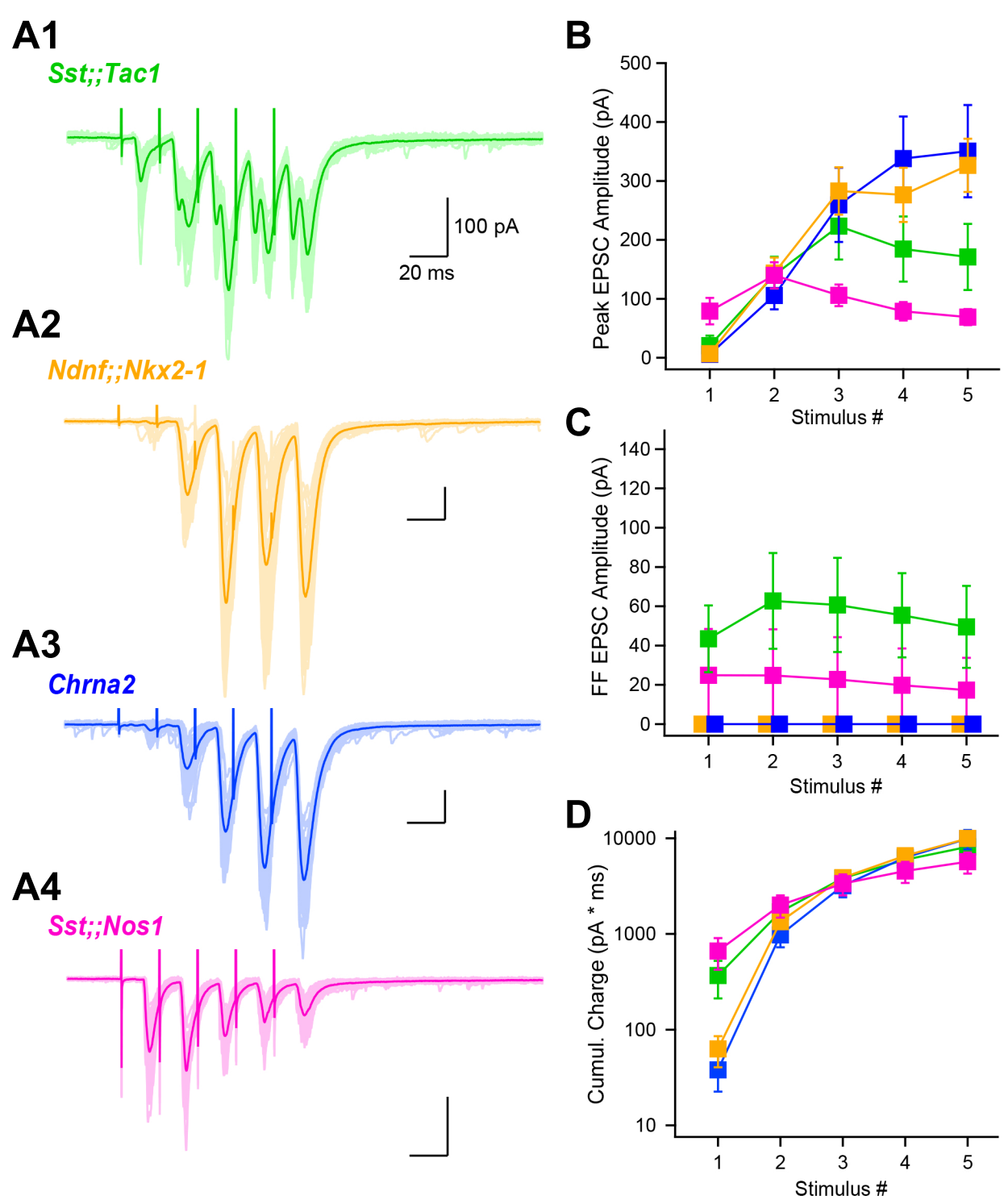

Supplementary Figure 14

Supplementary Table 1: p-values for statistical comparisons of anatomical parameters

p-values		*Sst*	*Sst;;Tac1*	*Ndnf;;Nkx2-1*	*Chrna2*
Axons	***Sst;;Tac1***	0.1679			
	Ndnf;;Nkx2-1	0.1200	0.7173		
	Chrna2	0.0549	0.0006	0.0033	
	Sst;;Nos1	0.0552	0.2769	0.0779	0.0404
Dendrites	***Sst;;Tac1***	0.0003			
	Ndnf;;Nkx2-1	1.0000	0.0000		
	Chrna2	1.0000	0.0011	1.0000	
	Sst;;Nos1	0.0013	1.0000	0.0001	0.0036

Supplementary Table 2: p-values for statistical comparisons of electrophysiological parameters

p-values		*Sst*	*Sst;;Tac1*	*Ndnf;;Nkx2-1*	*Chrna2*
ahp_max	***Sst***				
	Sst;;Tac1	1			
	Ndnf;;Nkx2-1	0.27131	0.46995		
	Chrna2	0.45678	1	0.05058	
	Sst;;Nos1	1	1	0.48616	1
ap_amp	***Sst***				
	Sst;;Tac1	0.00001			
	Ndnf;;Nkx2-1	0.21046	0.00231		
	Chrna2	0.17944	0.00002	0.65821	
	Sst;;Nos1	0.09317	0.65821	0.21046	0.01603
ap_thresh	***Sst***				
	Sst;;Tac1	0.03527			
	Ndnf;;Nkx2-1	0.58869	0.01127		
	Chrna2	0.41629	0.35321	0.35321	
	Sst;;Nos1	0.00010	0.06738	0.00014	0.00041
ap_fwhm	***Sst***				
	Sst;;Tac1	0.82730			
	Ndnf;;Nkx2-1	0.33143	0.33143		
	Chrna2	0.01216	0.05686	0.82730	
	Sst;;Nos1	0.00193	0.00043	0.00014	0.00009
sag	***Sst***				
	Sst;;Tac1	0.00772			
	Ndnf;;Nkx2-1	0.00021	0.00025		
	Chrna2	0.00001	0.00002	0.79104	
	Sst;;Nos1	0.00008	0.00943	0.00010	0.00007
ap_maxdecay	***Sst***				
	Sst;;Tac1	0.00438			
	Ndnf;;Nkx2-1	0.03824	0.03824		
	Chrna2	0.00438	0.00411	0.05446	
	Sst;;Nos1	0.00438	0.00438	0.00041	0.00009
ap_maxrise	***Sst***				
	Sst;;Tac1	0.00221			
	Ndnf;;Nkx2-1	0.44075	0.00046		
	Chrna2	0.20462	0.00015	0.18580	
	Sst;;Nos1	0.00593	0.20462	0.00221	0.00046
rebound dep	***Sst***				
	Sst;;Tac1	0.01608			
	Ndnf;;Nkx2-1	0.00010	0.00074		
	Chrna2	0.00001	0.00005	0.39715	
	Sst;;Nos1	0.00052	0.02695	0.00028	0.00015

Supplementary Table 3: Contribution of individual parameters to the principal components

	PC1_feat	PC2_feat	PC3_feat	PC4_feat	PC5_feat	PC6_feat	PC7_feat	PC8_feat
ap_thresh	0.38	0.39	0.30	0.44	0.37	0.37	0.37	0.11
ap_amp	0.14	0.24	0.50	0.17	0.44	0.21	0.25	0.59
ap_fwhm	0.56	0.03	0.13	0.04	0.18	0.42	0.49	0.47
ap_maxrise	0.08	0.63	0.47	0.34	0.05	0.40	0.18	0.27
ap_maxdecay	0.65	0.05	0.04	0.40	0.19	0.13	0.28	0.54
sag	0.21	0.00	0.16	0.08	0.14	0.66	0.64	0.23
rebound dep	0.23	0.54	0.19	0.69	0.32	0.14	0.15	0.06
ahp_max	0.08	0.33	0.60	0.13	0.69	0.10	0.12	0.01